We are IntechOpen, the world's leading publisher of Open Access books Built by scientists, for scientists

4,800
Open access books available

122,000
International authors and editors

135M
Downloads

Our authors are among the

154
Countries delivered to

TOP 1%
most cited scientists

12.2%
Contributors from top 500 universities

CLARIVATE ANALYTICS BOOK CITATION INDEX INDEXED

WEB OF SCIENCE™

Selection of our books indexed in the Book Citation Index in Web of Science™ Core Collection (BKCI)

Interested in publishing with us?
Contact book.department@intechopen.com

Numbers displayed above are based on latest data collected.
For more information visit www.intechopen.com

Chapter 7

Mechanism of Corrosion and Erosion Resistance of Plasma-Sprayed Nanostructured Coatings

Zaki Ahmad, Asad Ullah Khan, Robina Farooq, Tahir Saif and Naila Riaz Mastoi

Additional information is available at the end of the chapter

http://dx.doi.org/10.5772/64316

Abstract

There has been a dramatic increase in recent years in a demand for tough, wear-resistant, abrasion, erosion, and corrosion-resistant coatings for petroleum, chemical, aerospace industry, and processes encountering harsh environments such as paper and pulp equipment (the ball valve for high-pressure leaching). Whereas sufficient information on mechanical properties, such as abrasion, wear, and fatigue, has been gathered over the years, work on the resistance of these coatings to erosion and corrosion is seriously lacking. In the work reported, it has been shown that nanostructured TiO_2 coatings offer superior physical and mechanical properties compared to conventional TiO_2 coatings. Three different types of plasma-sprayed titanium dioxide coated samples on mild steel substrate were employed for investigation. The feedstocks used were Sulzer Metco nanopowders designated as AE 9340, AE 9342, and AE 9309. Powder 9340 was a precursor. The corrosion resistance of nanostructured TiO_2 coating was dictated largely by surface structure and morphology. The distribution and geometry of splat lamellae, contents of unmelted nanoparticles, and magnitude of porosity are the important factors that affect corrosion resistance. TiO_2 showed excellent resistance to corrosion in 3% NaCl. The maximum corrosion rate was observed to be 4 mils per year as shown by polarization potential and weight loss studies. The erosion-corrosion resistance of the plasma-sprayed nanostructured titanium dioxide coatings depends largely upon the characteristics of feed powder and its reconstitution. Dense, uniform, and evenly dispersed nanostructured constituents provide a high coating integrity, which offers high resistance to erosion-corrosion. A mechanism of erosion-corrosion is explained in the chapter with a schematic diagram. The findings show that the nanostructured TiO2 coatings offer superior resistance to corrosion, erosion, and environmental degradation.

Keywords: plasma air spray (PAS), nanostructured TiO_2 coating, inter-splat boundaries, fully melted particle zone, erosion corrosion

1. Introduction

Recent years have witnessed an increased demand for erosion-corrosion, wear, and abrasive resistant coatings for harsh environment in industry [1,2]. Thermal spray process of coating has brought a dramatic improvement in the quality of new generation TiO2 nanostructured coatings. A conventional thermal process is illustrated in **Figure 1**.

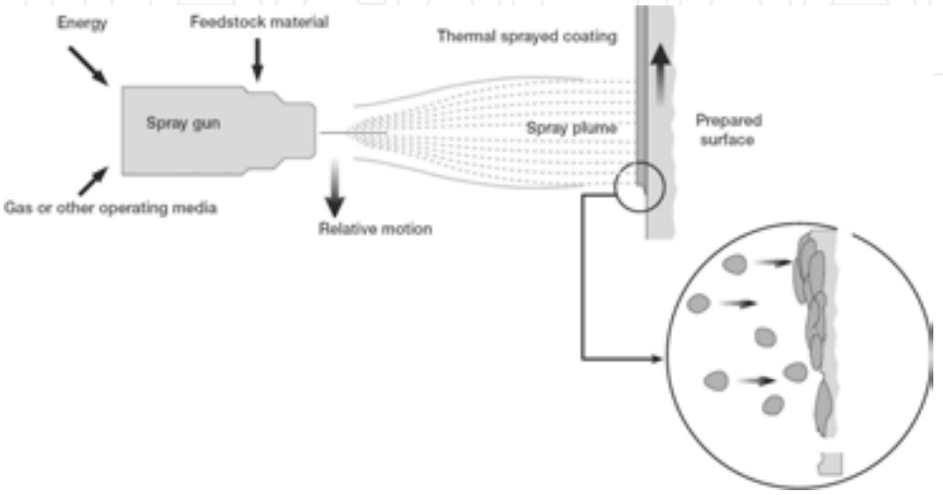

Figure 1. Thermal spray process principle. [Source: An Introduction to Thermal Spray, Issue 4 © 2013 Sulzer Metco].

TiO_2 coatings have been applied in harsh environments, gas sensors, paper and pulp industry, and electronic devices [3]. Thermal spray process has been very successfully used for application of bulk TiO_2 and nanostructured titanium dioxide coatings. A schematic diagram for thermal spray is shown in **Figure 2**. The unmelted particles, porosity, and oxide particles are shown in **Figure 2**. TiO_2 is highly stable, non-toxic, and bio-compatible. It shows a high dielectric constant and exhibits high photocatalytic activity. It is therefore used as an immobile catalyst in photocatalytic reactors [3–5]. It has been reported that nanostructured titanium dioxide coating exhibits a superior resistance to corrosion compared to conventional titanium dioxide coatings. The native oxide film of titanium dioxide (anatase) is about 2–10 nm thick which acts as a barrier for harsh environment. The thin film formed on anatase and rutile titanium dioxide is highly protective. It has been reported that nanostructured TiO_2 coatings offer superior physical and mechanical properties compared to conventional TiO_2 coatings [6]. Bansal et al. have characterized the interfacial microstructure, toughness, and failure modes in "conventional" and the "nano" Al_2O_3-13 wt% TiO_2 plasma-sprayed ceramic coatings [7]. There is evidence to show the advantages exhibited by nanostructured coatings due to their exceptional properties obtained if the crystalline character of the starting material is preserved [7]. The important consideration is to minimize coarsening of particles. Whereas a lot of work has been conducted on the physical and mechanical properties of nano-TiO2 coatings, the work on corrosion and erosion resistance is scarce. Hence, an attempt has been made to fill this gap by evaluating the erosion-corrosion and corrosion resistance of bulk and nanostructured titanium dioxide coatings by different techniques.

http://dx.doi.org/10.5772/64316

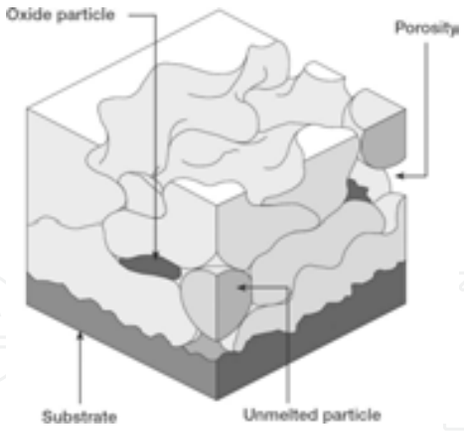

Figure 2. Thermal-sprayed coating schematic diagram. [Source: An Introduction to Thermal Spray, Issue 4 © 2013 Sulzer Metco].

2. Experimental

Investigations were conducted on three different types of titanium dioxide plasma-sprayed samples. These samples were numbered as M102, AE9342, and AE9303 for identification. Sample M102 was prepared from bulk titanium dioxide and plasma sprayed. It was used as a control sample for comparison.

2.1. Nano feedstock

Nano feedstocks obtained from Sulzer Metco are numbered as AE9340, AE9342, and AE9303 for identification. Feedstock AE9340 acted as a precursor. It was spray dried from powder AE9340 by feeding it through a plasma flame. This procedure reduced the volume and increased the density of the powder. Powder AE9303 was made by combination and spray drying technology followed by sintering. The structural features of the powder are shown in **Figures 3–5**.

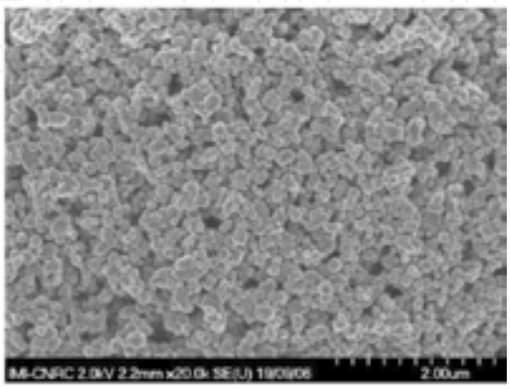

Figure 3. SEM image of spray-dried AE9340 nanopowder (METCO). [Source: Ahmad and Ahsan [8]].

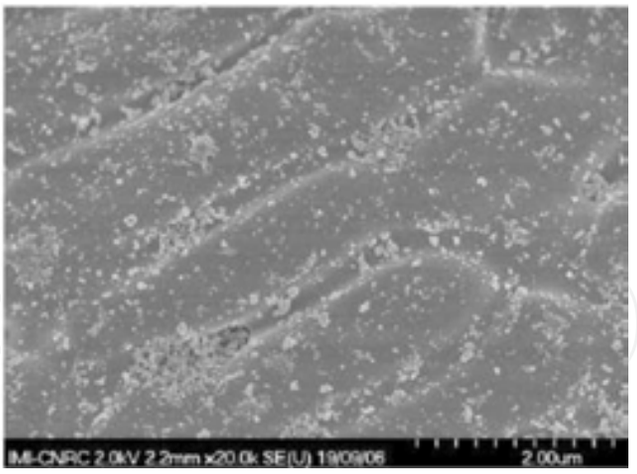

Figure 4. SEM image of spray-dried and densified nanopowder supplied by Sulzer Metco. [Source: Ahmad and Ahsan [8]].

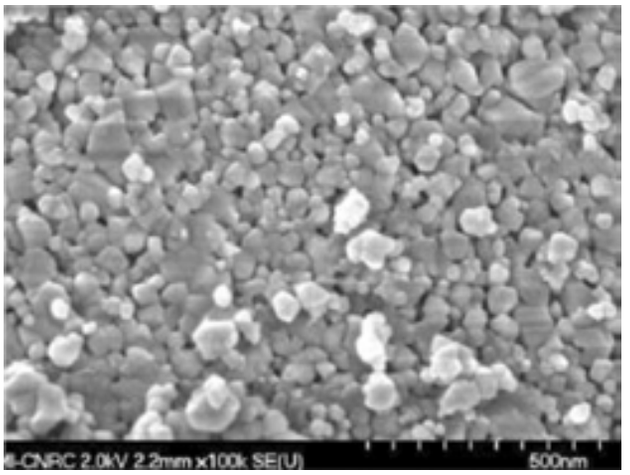

Figure 5. SEM image of nanopowder, spray dried and sintered supplied by Sulzer METCO. [Source: Ahmad and Ahsan [8]].

The interfacial thickness of the "conventional" and the "nano" Al_2O_3-13 wt% TiO_2 plasma coating in steel substrate has a significant effect on the bond distance. The Rockwell hardness of conventional and nanostructured coating was found to be 22 and 45 J/m^2 respectively. The micro structure of the conventional coating consisted of fully molten and solidified splats. The nano coating showed regions of fully molten (FM) splats, interspersed with partially molten rounded feature. One important observation was weak adhesion of partially melted/steel interface which cracked, whereas fully molten interface of splats showed no cracking and complete adhesion to the substrate. In a work by Shaw et al., it was found that the coatings produced from nano feedstock showed better resistance than the coating produced from commercial coarse grade powders [9]. Similarly, it was found that the zirconia nanostructured coatings showed better performance than their conventional counterpart. Their superiority was attributed to optimized microstructure and improved microhardness. Detailed studies

http://dx.doi.org/10.5772/64316

were performed on microstructural properties, abrasive and sliding wear. Atmospheric plasma spraying and vacuum plasma spraying on Al_2O_3, 13 TiO_2, Cr_2O_3-5-SiO_2-3 TiO_2, and TiO_2 coatings [10].

The VPS-coated surface showed improved properties because the coatings retained a typical structure which was composed of both fully melted and partially melted particles.

In general, the physical and mechanical properties of nanostructured coatings showed improved mechanical properties, low density, improved hardness, ideal adhesion strength, strong resistance to crack growth, and strong resistance to spalling. The above-mentioned properties suggest a beneficial effect of using nanopowder for fabrication of plasma-sprayed nanostructural surface. Despite the progress made, studies on corrosion are seriously lacking in this area.

Harsh environments are encountered in service such as pulp and paper industry and similar other industries. Resistance to erosion-corrosion is crucial to the integrity of the coating. Unfortunately, information on the mechanism of erosion-corrosion and localized corrosion is very scarce. An attempt has been made for reporting corrosion behavior of nano titanium dioxide plasma-sprayed coatings in this article.

2.2. Process

A patented plasma spray coating procedure invented by Sulzer Metco was used to coat the sample. The nanopowder was fed by argon, hydrogen and helium. The slurry composed of binder, nanopowder, and solvent was fed at a rate of 25 l/min by a peristaltic pump. A 9 MB plasma gun was used in the procedure. Argon gas carried the powder at a feed rate of 14 g/L in the plasma jet generated from argon at ~40 spm and 2–3 rpm. A constant current was maintained at 400 A. The process is shown in **Figure 6**.

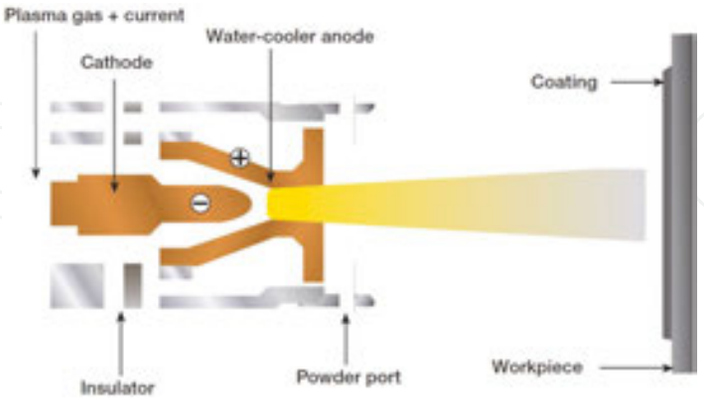

Figure 6. Illustrative diagram of plasma spray process. [Source: An Introduction to Thermal Spray, Issue 4 © 2013 Sulzer Metco].

In the high-velocity oxy-fuel process, **Figure 7**, Sulzer Metco CDS100 gun was utilized. The flame was produced by combustion of oxygen and methane. The flame temperature was

lowered by nitrogen. The feed rate was 20 g/L at a flow rate of 12 spm. The spray distance was maintained at 100 mm.

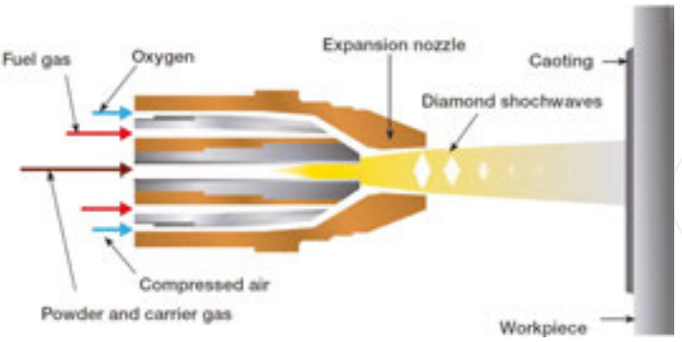

Figure 7. High-velocity oxy-fuel spray process diagram. [Source: An Introduction to Thermal Spray, Issue 4 © 2013 Sulzer Metco, with kind permission of Sulzer Metco].

2.3. Specimen preparation

The sample thickness was 0.033 mm and it was coated only on one side. A commercial bond coat was applied on both sides of the sample to protect their surface. The sides were sealed by paint. The sample was exposed to a wet grinding machine with 320 and 600 grit SiC paper. Water was used as a lubricant. The size of the samples was 70 × 100 mm, 58 × 100 mm, 48 × 100 mm, and 40 × 100 mm in dimension for fitting in holder of the loop. A schematic diagram of the loop is shown in **Figure 8**.

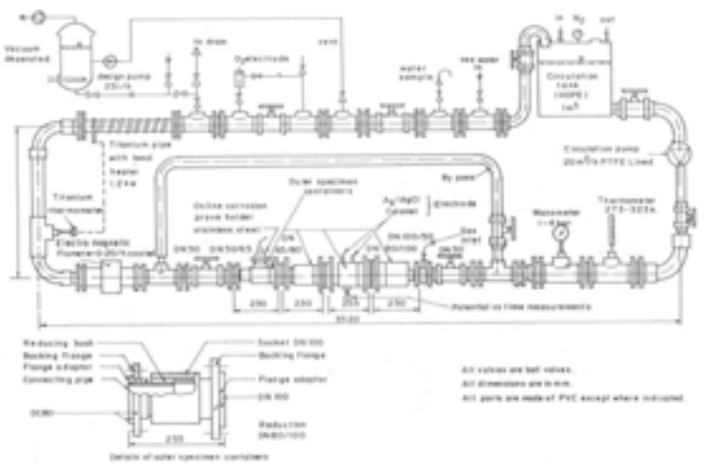

Figure 8. A custom-designed PVC loop for erosion-corrosion study. [Source: Ahmad and Aleem [11]].

2.4. Microanalytical studies

The surface morphology of the sample was examined by a low vacuum scanning electron microscope. An energy-dispersive oxford system was used for elemental analysis. Nano-R2

http://dx.doi.org/10.5772/64316

atomic force microscope was used for the study of surface morphology in contact and vibrational mode.

2.5. Recirculation loop

Erosion-corrosion studies were conducted by a high-density custom-designed PVC loop. The main parts of the loop consisted of entry and exit control valve, manometer, water pump, flow meters, and sample holders of different sizes. The loop comprised two columns, each column capable of holding six specimen holders and each specimen holder had a capacity to accommodate six specimens. The samples fixed on the holders were exposed to velocity ranging from 1.0 m/s to 4 m/s. The temperature in the loop was 45±2°C. The loop was run for 150 h at one time.

2.6. Immersion tests

Laboratory immersion was conducted according to ASTMG31 [12]. Before exposing the samples to 3.5 wt% NaCl, they were cleaned with acetone and rinsed with distilled water. The samples after exposure were dried and put in a desiccator. The rate of corrosion was determined by the loss in the weight of the samples after immersion.

2.7. Electrochemical studies

Electrochemical polarization resistance [13] measurements were made in accordance with recommendations of ASTM G59 after immersing them for 2 hours to obtain equilibrium and applying a controlled potential scan over a range of ± 25 mV with respect to corrosion potential (Ecorr). Software supplied by Gamry was used and the data were recorded. On processing, the following corrosion rates were achieved (**Figure 9**).

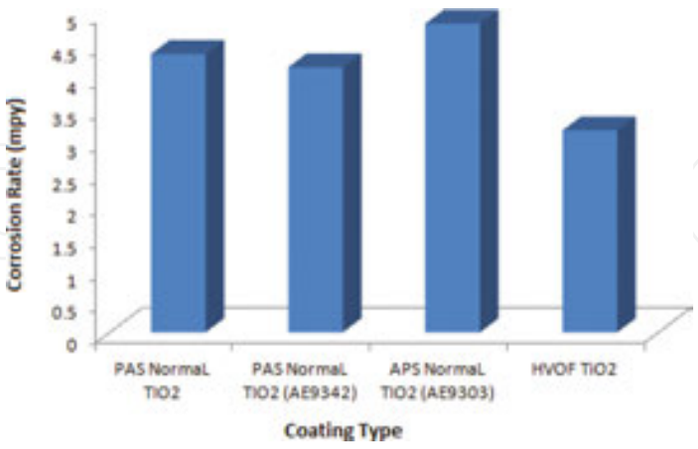

Figure 9. Corrosion rates of nanostructured and conventional titanium oxide coatings by salt spray chamber test. [Source: Ahmad and Ahsan [8]].

The polarization resistance diagrams are shown in **Figures 10–12**. It is clearly observed that the least rate of corrosion is exhibited by HVOF-coated sample followed by the AE9342

(nanostructured TiO_2 coated), the polarization resistance of the two samples being 1.404 ohms and 1.147 ohms, respectively. This is consistent with the morphology of the splats which shows a large region of fully melted particles homogeneously distributed compared to others with voids, agglomerates, large number of splat boundaries which creates conditions for the onset of corrosion. The morphology would be discussed more under the section of erosion-corrosion.

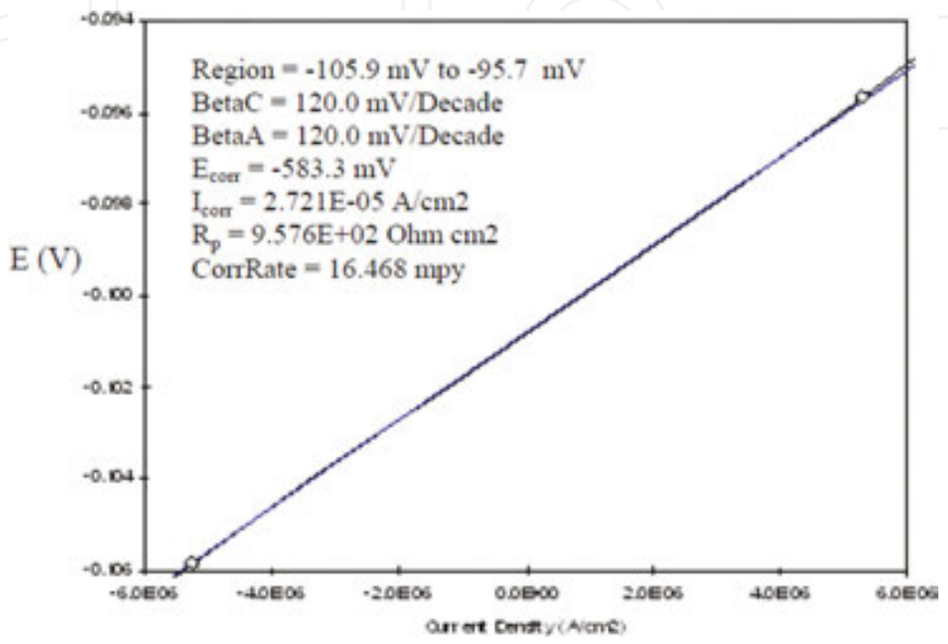

Figure 10. A polarization resistance plot of TiO2-coated specimen in 3.5% NaCl. [Source: Ahmad and Ahsan [8]].

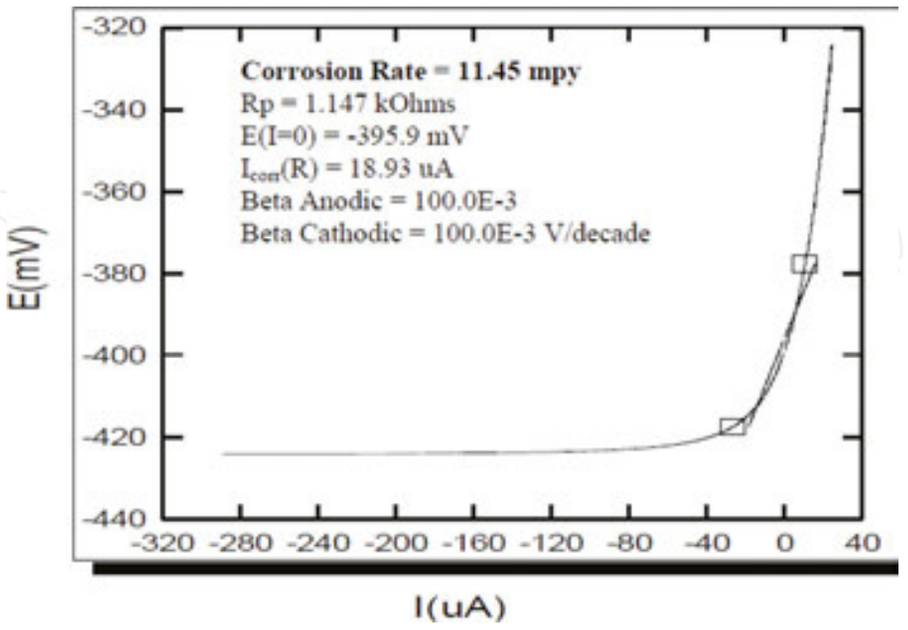

Figure 11. Polarization resistance curve for nano TiO2-coated specimen (AE9342). [Source: Ahmad and Ahsan [8]].

http://dx.doi.org/10.5772/64316

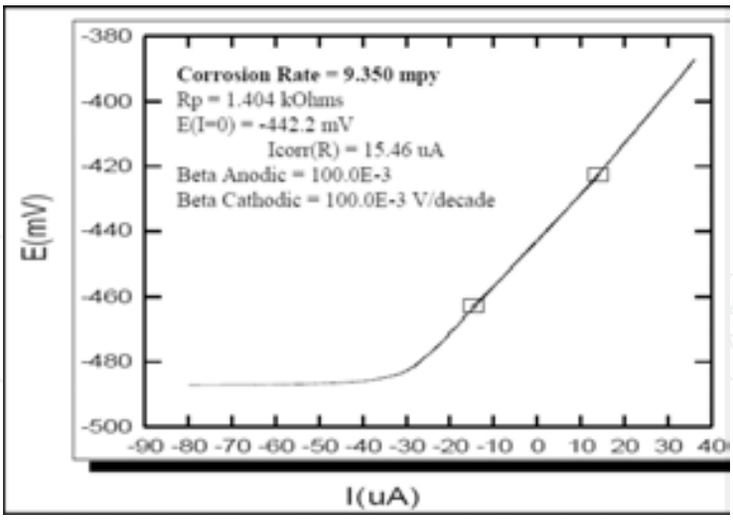

Figure 12. A polarization resistance plot of TiO_2-coated specimen by HVOF. [Source: Ahmad and Ahsan [8]].

2.8. Salt spray studies

Salt spray tests were conducted as per ASTM B117 [14]. The corrosion rate of samples exposed to salt spray for 1000 hours is shown in **Figure 13**. There is no significant difference in the rate of corrosion as the TiO_2-coated specimens are in general highly resistant to humid conditions and salt water. However, the nanostructured coating exhibits slight superiority to the normal TiO_2 (4.143739 and 4.846697 mpy) vs. 4.3519 mpy, respectively. A slightly higher resistance is shown by the HVOF-coated sample (3.157205 mpy). The difference can be attributed to morphological variations which affect the integrity of coating.

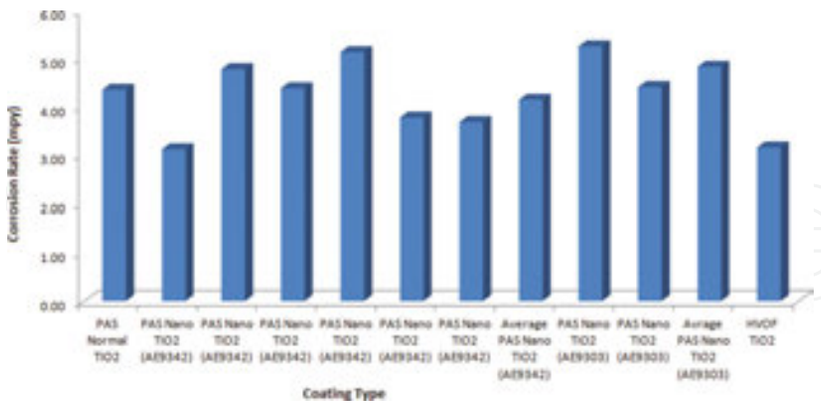

Figure 13. Corrosion rates of nanostructured and conventional titanium oxide coatings by salt spray chamber test. [Source: Ahmad and Ahsan [15]].

2.9. The erosion-corrosion studies

The erosion-corrosion resistance of the coated samples was determined in a high-density PVC recirculating loop described in the experimental section. At lower velocities (1 m/s), only a

slight damage was observed on the TiO_2-coated specimens. Localized corrosion such as galvanic and crevice attack was observed. Surface etching by impact of polystyrene NaCl slurry occurs preferentially in the splat boundaries. Narrow splat boundaries permit the penetration of eroded particles in solution, whereas wider boundaries in conventional coatings are more sensitive to erosion and water penetration. The surface morphology of the coating and homogeneous distribution of fully melted particles controls the degree of penetration. If water reaches the inter-splat boundaries, it reacts with the steel substrate and dislodges the iron particles with the subsequent formation of a fibrous network mainly composed of small particles of iron due to the interaction with slurry. Some oxide inclusions formed by reduction of traces of oxides for example Cr_2O_3 may participate with the formation of network.

In the conventional titanium dioxide coating, preferred dissolution of inter-splat boundaries is observed. The figure shows mixed splat geometry of specimen AE9342. A mixed geometry showing nano agglomerates, splats, and fully melted particles is shown in **Figure 14**. The morphological defects are shown in the figure with experimental analysis.

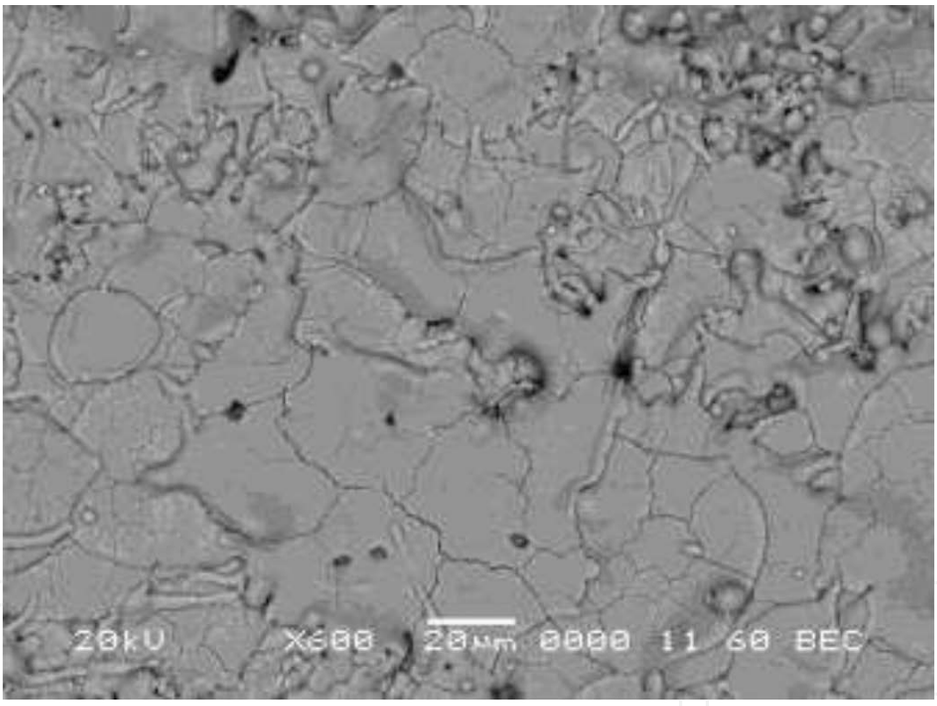

Figure 14. A homogenous surface morphology of AE9342 n-TiO2-coated specimen shows the densification of pancake-shaped splats. [Source: Ahmad and Ahsan [8]].

2.10. The fibrous network

The fibrous network may be attributed to the transpassiveness of the Fe particle from the substrate due to attack by slurry composed of polystyrene particles in 3.5 wt% NaCl solution. From experimental studies, it appears that dissolution by erosion-corrosion occurs mainly by the penetrating water in splat boundaries as shown in **Figure 15**.

http://dx.doi.org/10.5772/64316

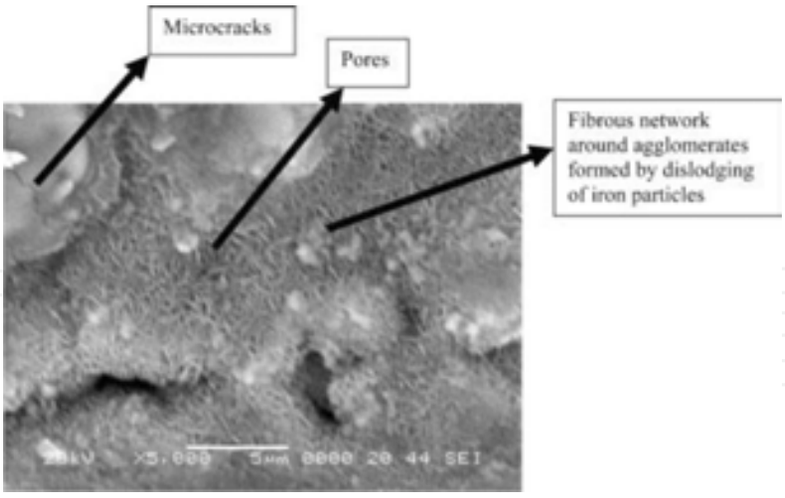

Figure 15. SEM image showing formation of fibrous network by dislodging of particles. [Source: Ahmad and Aleem [11]].

On comparing specimens AE9303 and AE9342, it is observed that the surface morphology of AE9303 is relatively nonuniform and has less number of splats. It also shows a smaller number of splat zones of fully melted particles. The above factors clearly show that the surface morphology controls the dissolution by erosion-corrosion. Specimen AE9303 offers a higher resistance.

The higher resistance of AE9342 nanostructured TiO2 PAS coated is further confirmed by the observation that the surface morphology of AE9342 reveals no corrosion attack on the splat grain boundaries, microgrooves, and spherical agglomerates. The dense, thick, and uniform morphology of AE9342 is shown in **Figure 16**.

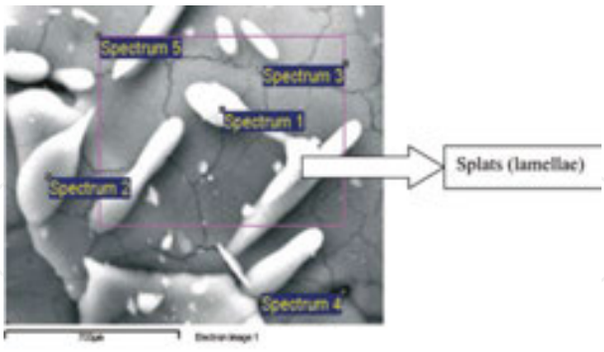

Processing option : All elements analyzed (Normalised)

Spectrum	O	Ti	Total
Spectrum 1	52.23	47.77	100.00
Spectrum 2	51.33	48.67	100.00
Spectrum 3	39.82	60.18	100.00
Spectrum 4	13.14	86.86	100.00
Spectrum 5	48.73	51.27	100.00
Max.	52.23	86.86	
Min.	13.14	47.77	

All results in Weight Percent

Figure 16. SEM image of specimen 9342 showing morphology of splats (lamellae). [Source: Ahmad and Aleem [11]].

2.11. Morphological studies

The microstructural features of nano-spray dried powders AE9340 and AE9342 (nano-spray dried and densified) followed by sintering were studied under low vacuum scanning electron microscope. The agglomerates formed from individual nanopowders are shown in **Figures 1–3**. Both powders exhibit granule shape which is mostly circular and devoid of small agglomerates glued to larger particle. The coating comprises mostly of melted nanoparticles which upon impingement on the substrate form splats. The partially melted particles can also be observed in the figure. A typical thermal monolithic coating would consist of non-homogeneous features including fine grain, splat boundaries, pores, inclusions, fully and partially melted and unmelted particles.

The morphology of coated specimens is shown in **Figures 17–21**. Specimen ME102 (control sample) exhibits unsymmetrical morphology pores, particles, nano unmelted particles, agglomerates of nano particles, and a zone of fully melted particles. For a plasma-sprayed coating to be ideal, it must show a large zone of fully melted particles. Specimen 9342 shows a zone of uniform distribution of fully melted particles compared to M102 which reveals the improved performance of TiO2 coating from nanopowder feedstock. In contrast, specimen AE9303 shows mixed splat geometry as a nonuniform distribution of splats (**Figures 22** and **23**). In HVOF-coated n-TiO2 specimens, a larger zone was observed to be covered with agglomerates of fully melted splat particles compared to plasma air-sprayed coating which offers it a slight superiority (**Figure 24**).

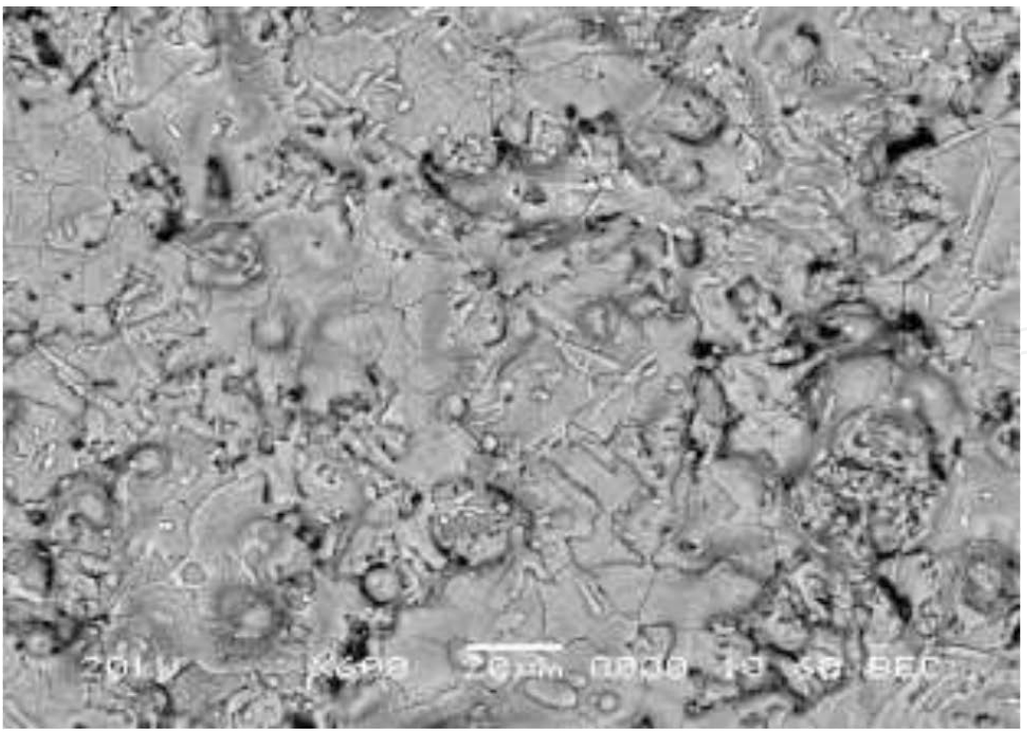

Figure 17. SEM image showing the state of splats as a dense structure in M102 (conventional TiO_2). [Source: Ahmad and Ahsan [8]].

http://dx.doi.org/10.5772/64316

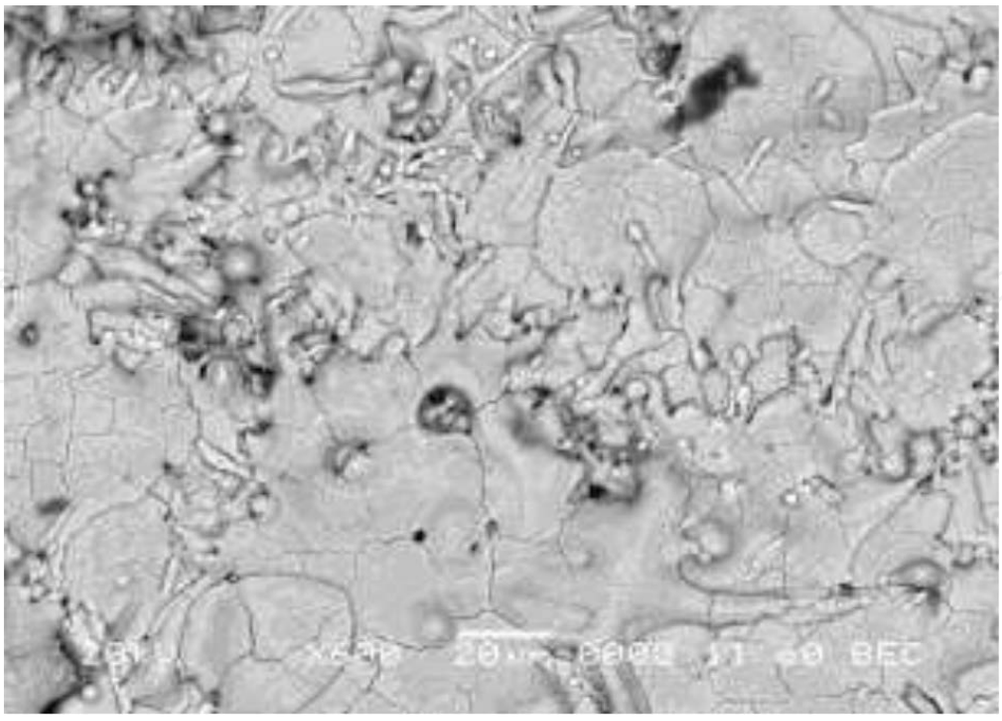

Figure 18. SEM image showing spherical pancake-shaped splats and pores in n-TiO_2 coating as observed in specimen in AE9342. [Source: Ahmad and Ahsan [8]].

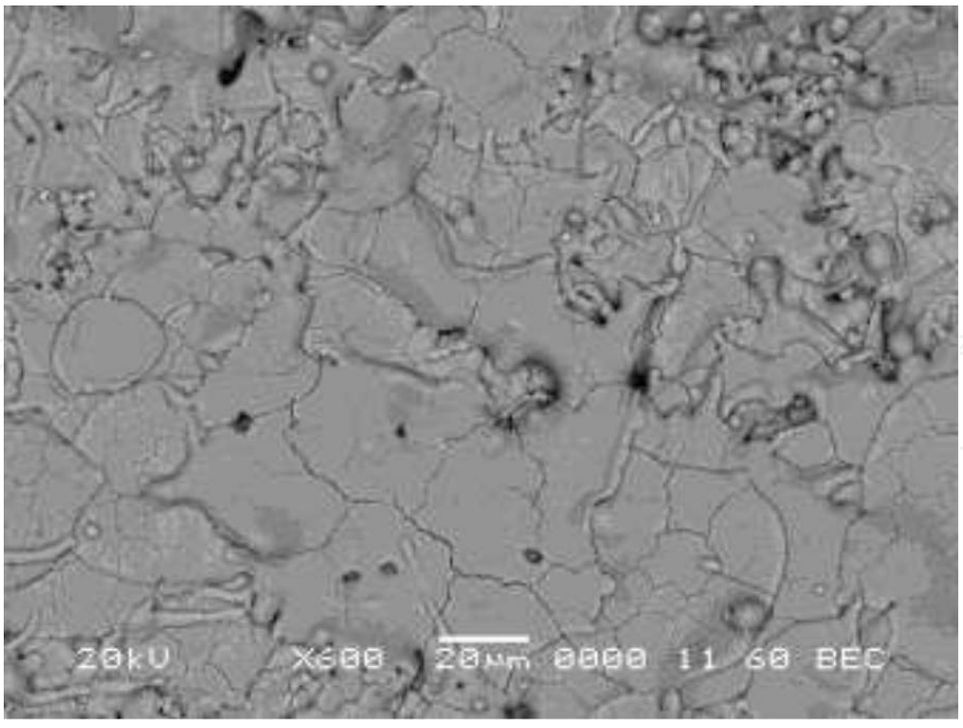

Figure 19. SEM image of n-TiO_2 coating on specimen AE9342 showing a high density of splats. [Source: Ahmad and Ahsan [8]].

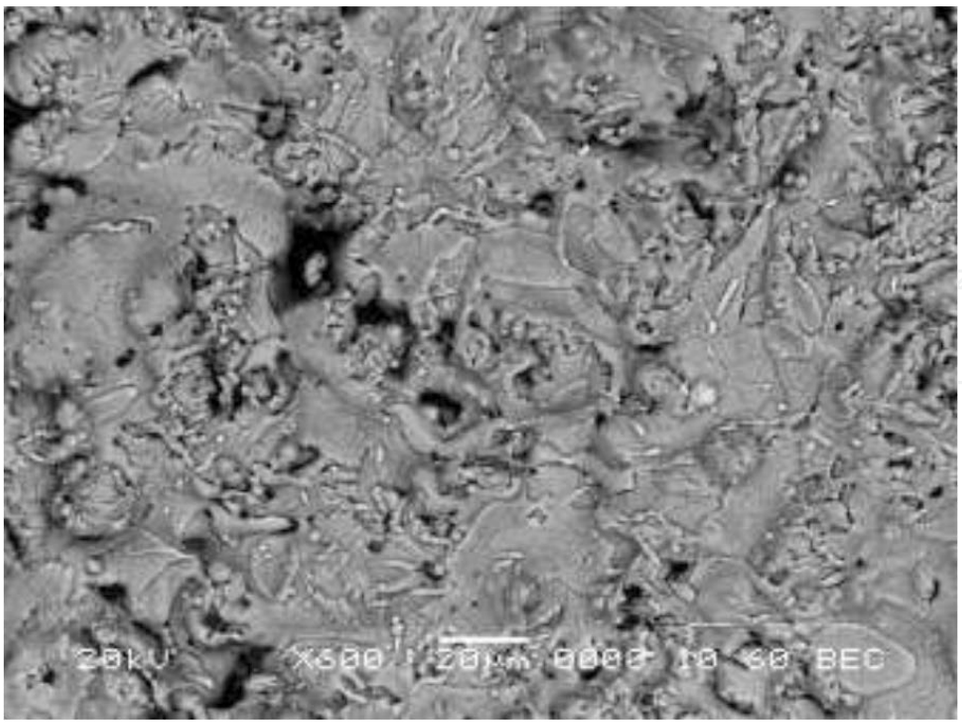

Figure 20. SEM image showing unmelted particles and pores on the surface of nano-TiO_2-coated specimen AE9342. [Source: Ahmad and Ahsan [8]].

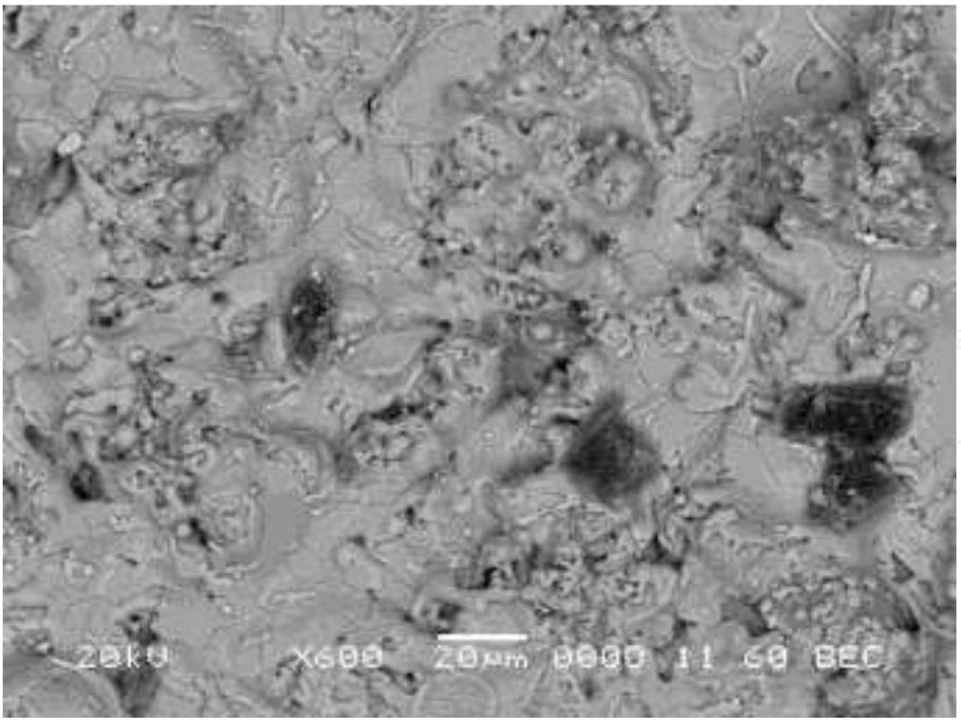

Figure 21. SEM image showing agglomeration of nanoparticles and zones of fully melted particles in AE9342. [Source: Ahmad and Ahsan [8]].

http://dx.doi.org/10.5772/64316

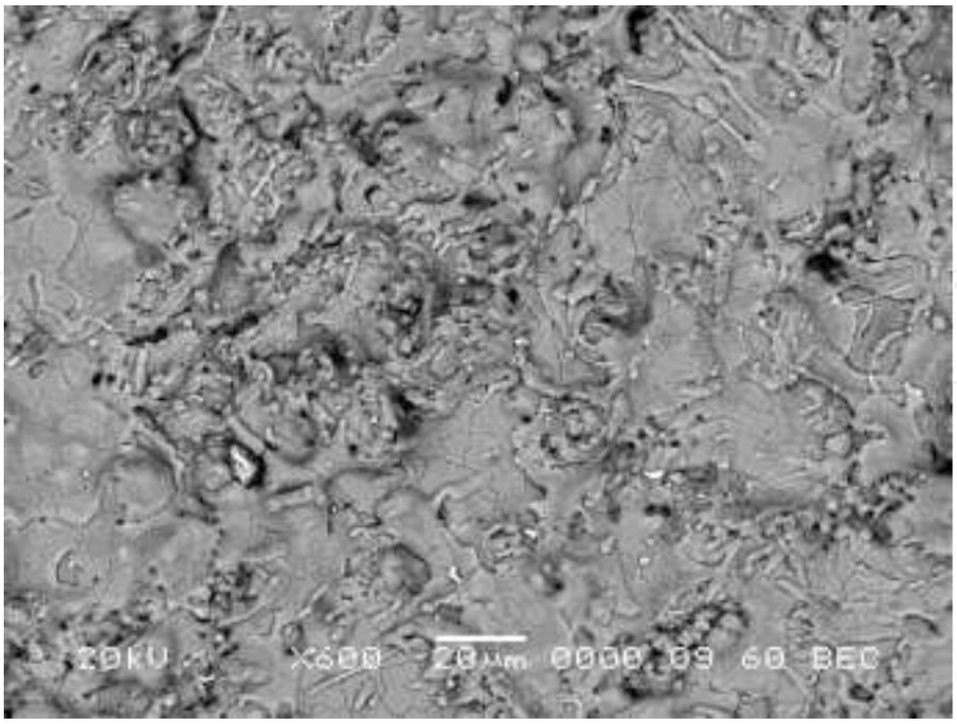

Figure 22. SEM image showing a nonuniform distribution of splats on sample AE9303. [Source: Ahmad and Ahsan [8]].

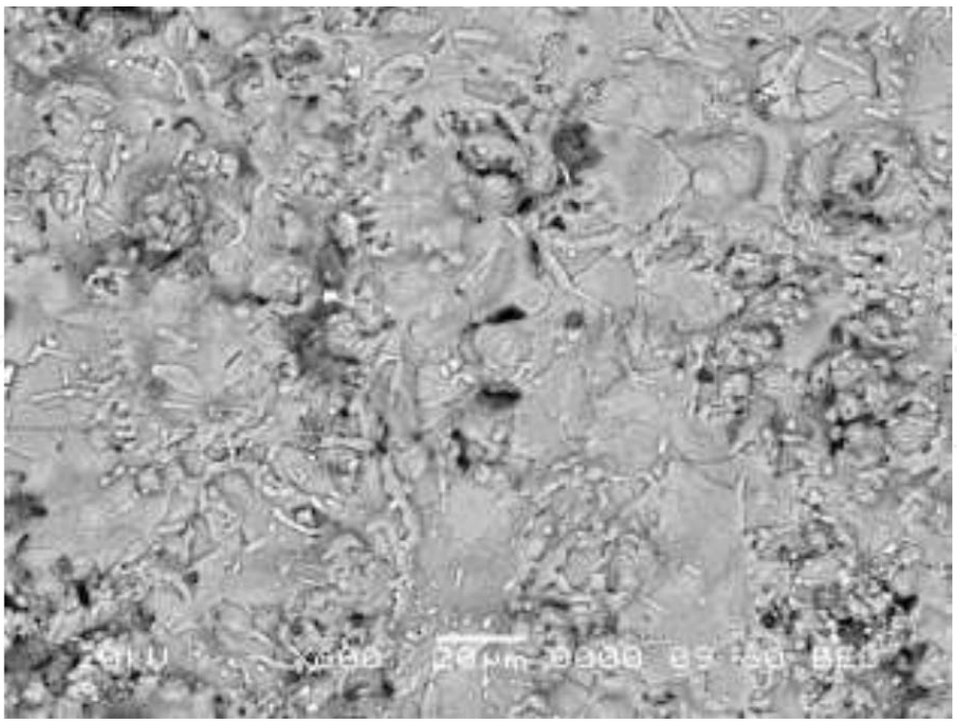

Figure 23. SEM image showing different shapes of splats, voids, and nonuniform surface on specimen AE9303. [Source: Ahmad and Ahsan [8]].

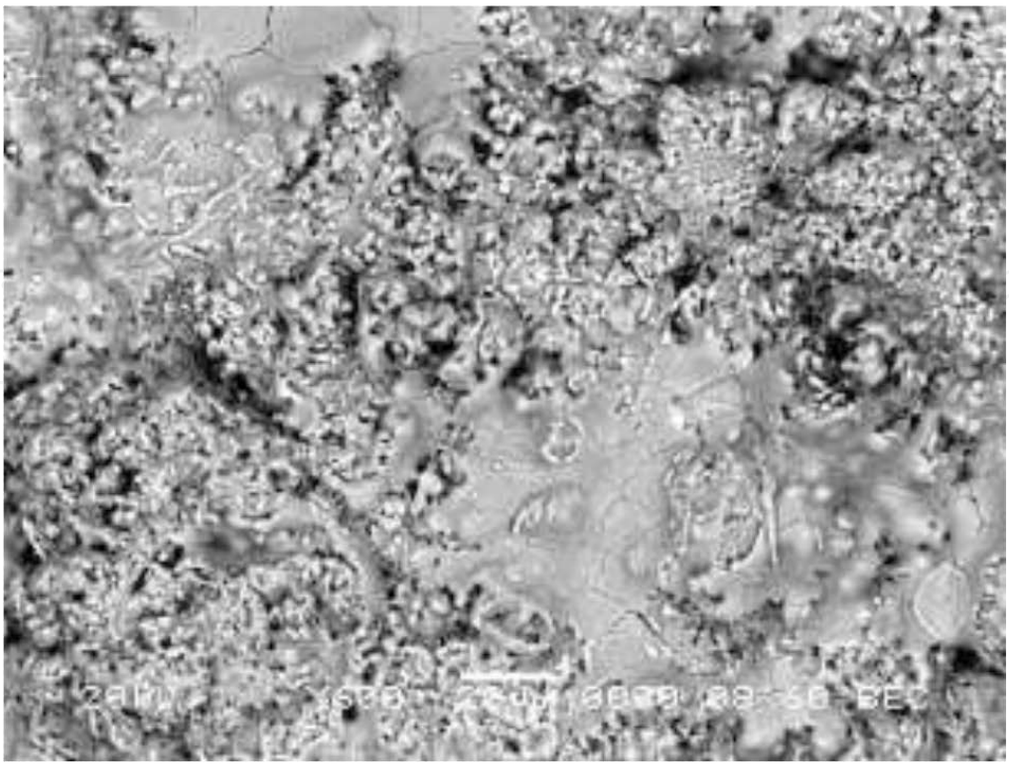

Figure 24. SEM image of HVOF-coated n-TiO_2, showing a large melted zone, uniform distribution of agglomerates, and a high density of melted particles. [Source: Ahmad and Ahsan [8]].

Different geometries of molten splats are shown in **Figure 25**. The AFM images of plasma air-sprayed coatings are shown in **Figures 26–32**. A layered structure with periodicity can be observed from smaller M102 (control sample). The horizontal shaped large voids and packing of splats can be observed in **Figures 29** and **30**. Specimen AE9342 exhibits grain boundaries, columnar grains, and a large zone of fully melted splats (**Figure 31**) and withstands erosion and corrosion. Morphological studies reveal that n-TiO_2-coated specimen possesses morphology critical to the beneficial properties of PAS TiO_2-coated substrate in steel. The magnitude of erosion-corrosion is higher in n-TiO_2 and AE9303 caused by dislodging of iron particles and an uneven nonhomogeneous-coated surface covered with a fibrous network of fragmented oxides. The dislodging of iron particles appears mainly to be responsible for the sensitivity of the substrate due to water penetration through the narrow splat boundaries to erosion-corrosion. The variation of corrosion rates with the velocity of the sample is shown in **Figure 33**. The increased corrosion rate has been attributed to the destruction of the passive layer unlike on the steel surface. The surface roughness of n-TiO_2 does not impede the development on the steel surface like in MMC (Metal Matrix Composite) where protrusion and particulate size increase the surface roughness with the range (20–30 μ) which allows ingress of slurry. This phenomenon is not conclusively understood. The impact of polystyrene NaCl slurry may cause a significant damage to MMCs because of protrusion of particles. It has been observed in the investigation that micro hardness of AE9342 has a greater homogeneity than AE9303 in the range of 36–58 nm which does not allow the ingress of slurry particles [11].

http://dx.doi.org/10.5772/64316

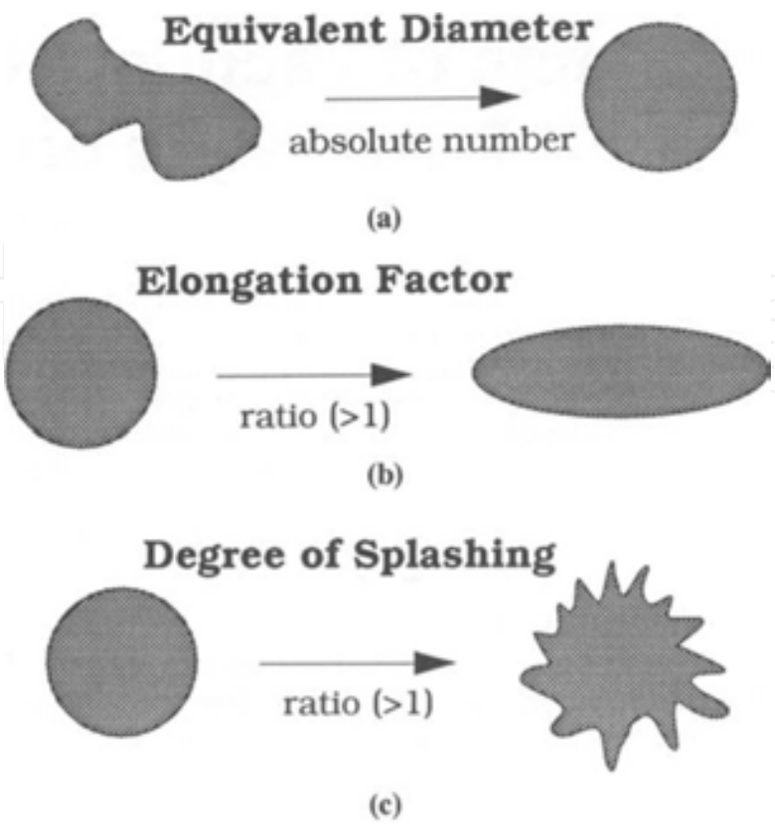

Figure 25. Figure showing the effect of absolute number, elongation, and degree of splashing on the shapes of splats. [Source: Montavon et al. [16]].

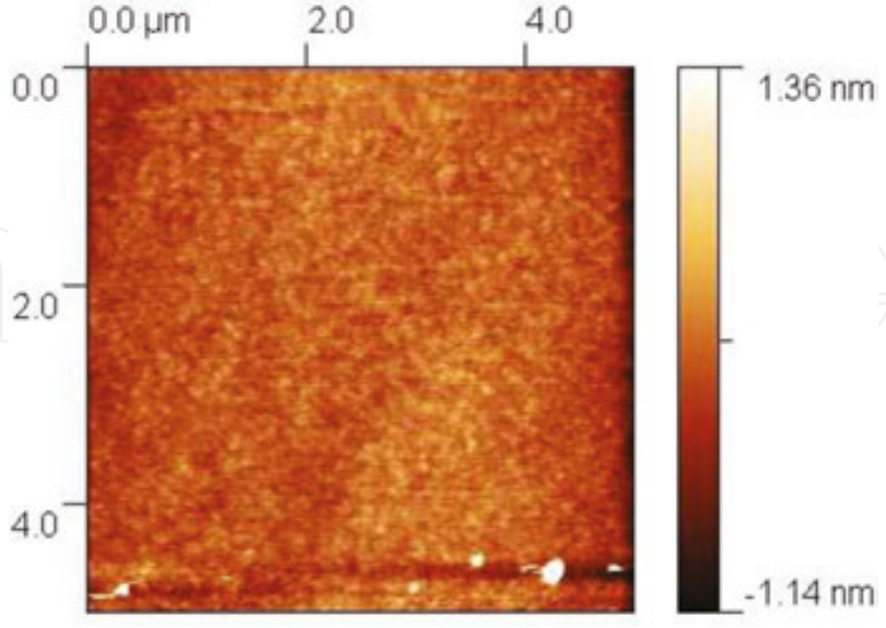

Figure 26. A layered structure imaging is observed in the AFM image of specimen M102. [Source: Ahmad and Ahsan [8]].

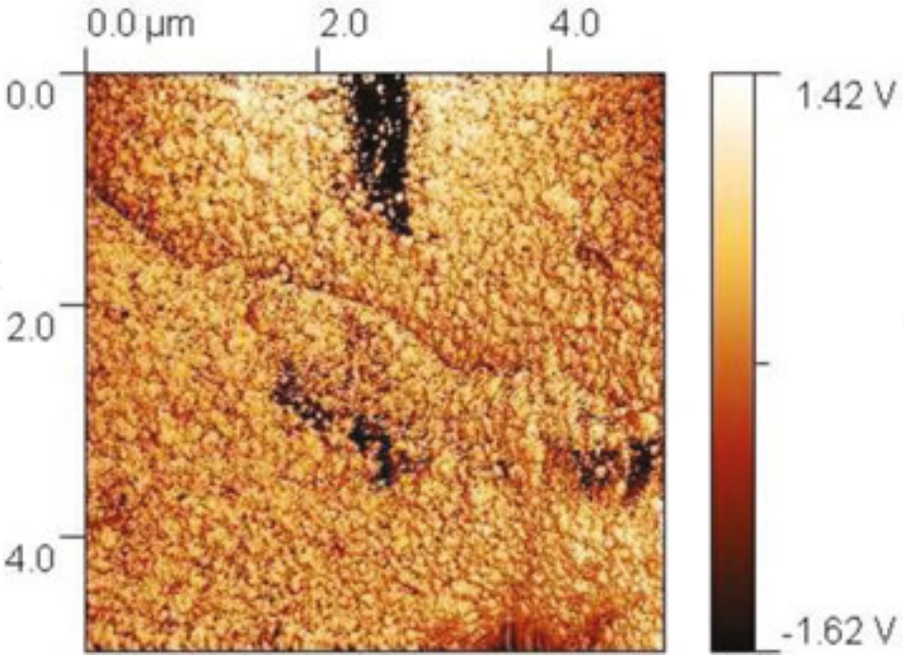

Figure 27. A dense and spherical topography is observed in the surface of specimen M102 in the vibration mode. [Source: Ahmad and Ahsan [8]].

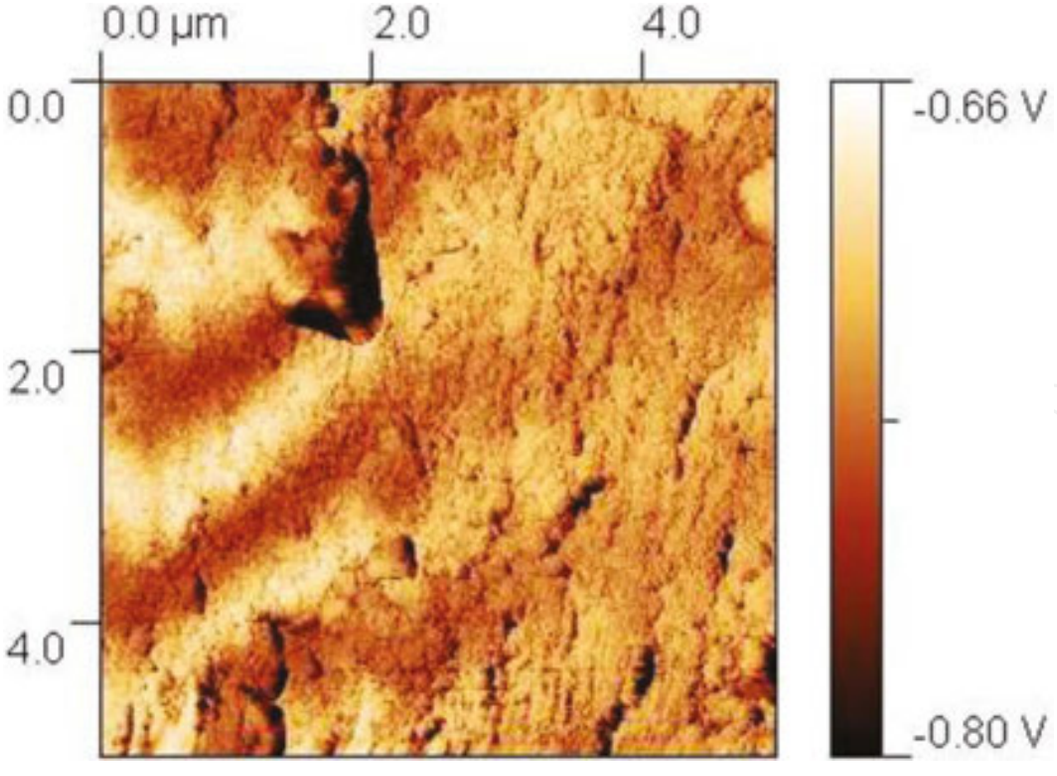

Figure 28. AFM topography of ME102 showing the repetition of fully melted and partially melted zones. [Source: Ahmad and Ahsan [8]].

http://dx.doi.org/10.5772/64316

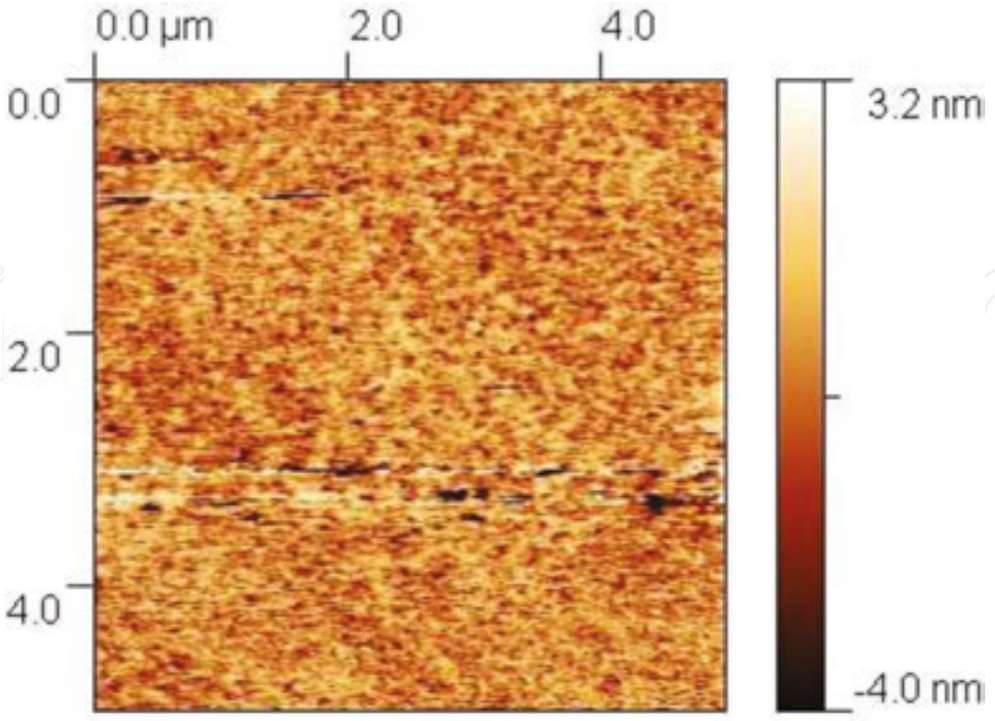

Figure 29. An AFM image showing morphology of specimen AE9303 in contact mode. [Source: Ahmad and Ahsan [8]].

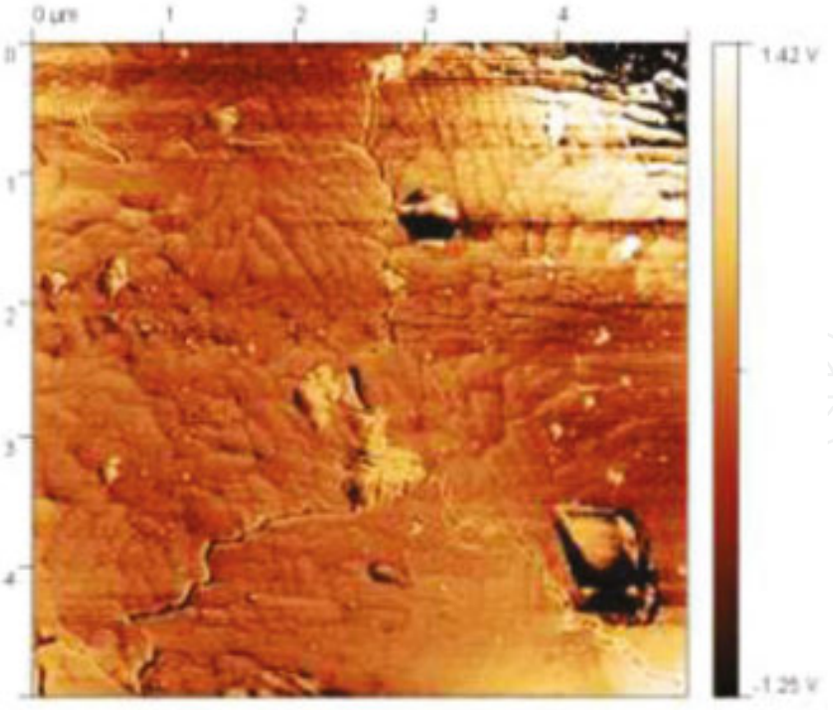

Figure 30. AFM image of AE9303 showing large voids and inter-splat zones in vibrating mode. [Source: Ahmad and Ahsan [8]].

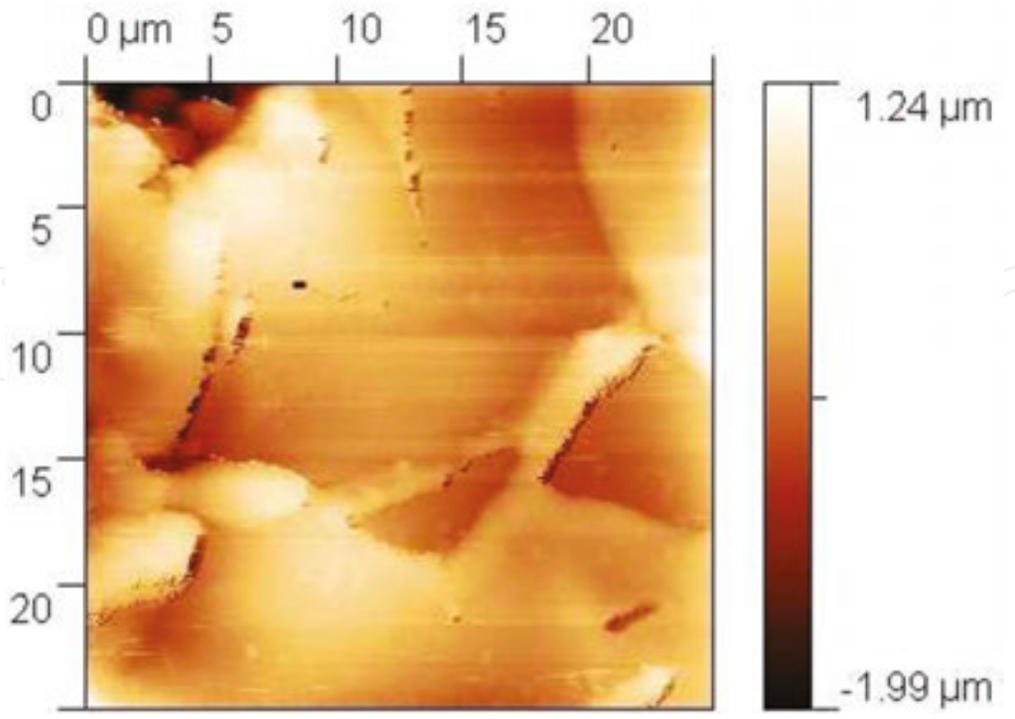

Figure 31. The grain boundaries of specimen AE9342 are clearly shown by AFM in contact mode. [Source: Ahmad and Ahsan [8]].

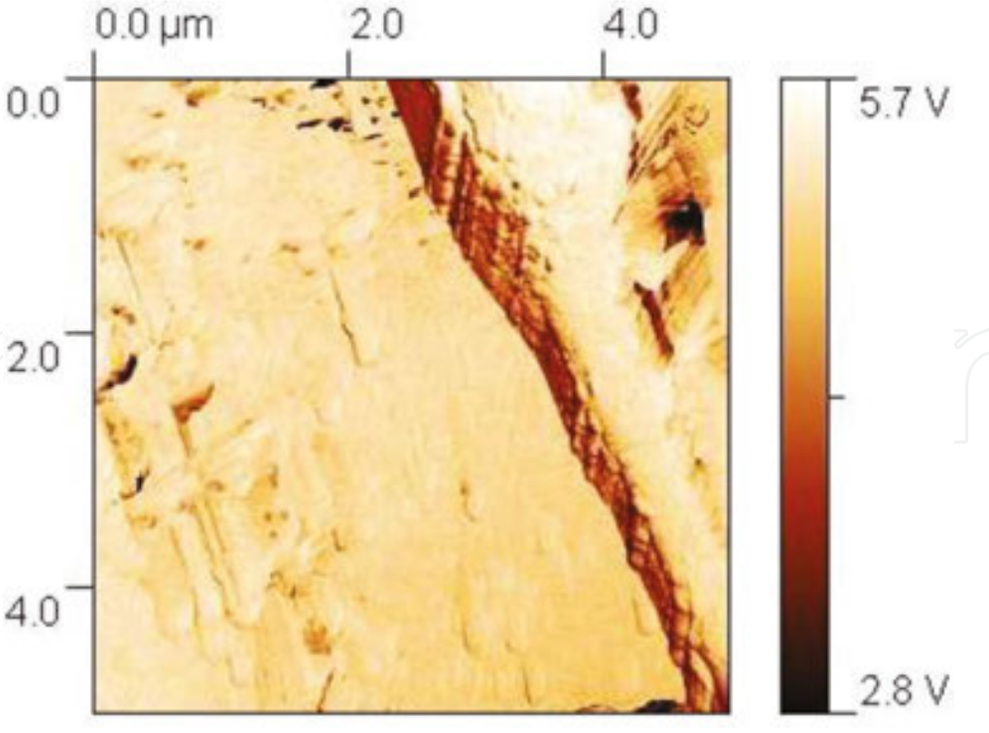

Figure 32. An AFM image of AE9342 in vibrating mode clearly showing distinct columnar grains. [Source: Ahmad and Ahsan [8]].

http://dx.doi.org/10.5772/64316

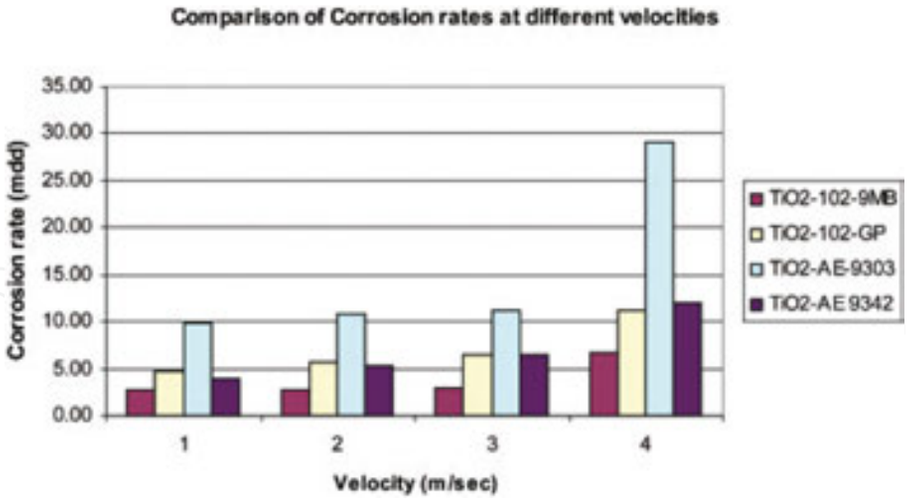

Figure 33. The effect of velocity on the corrosion rate of different alloys used in experiments showing the superior resistance of AE9342. [Source: Ahmad and Aleem [11]].

Erosion-corrosion of n-TiO_2-coated stainless steel by PAS is only confined to areas of heterogeneity. In conventional ceramic coatings, hardness of the coating has an inverse relationship with metal wastage, and resistance to erosion-corrosion is correlated with the composition and microstructure of coatings [17].

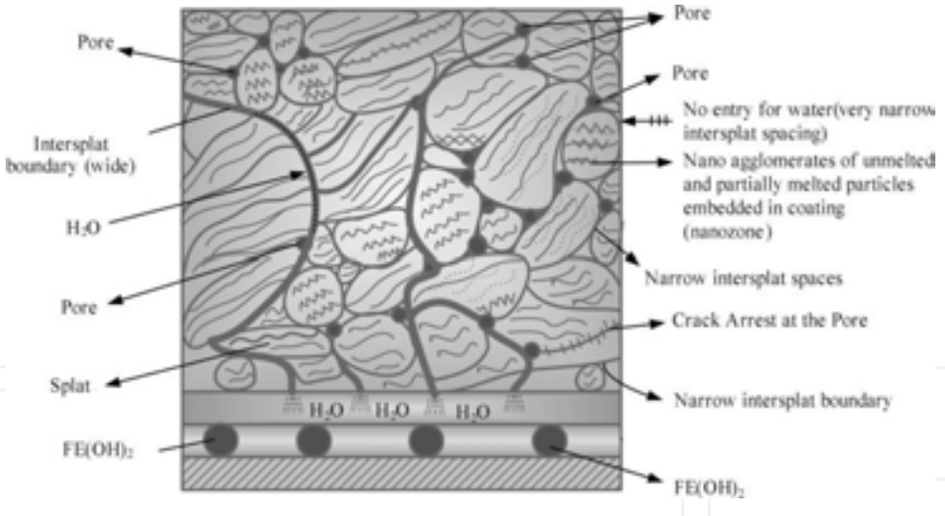

Figure 34. A schematic illustrating the mechanism of erosion-corrosion of plasma spray coated surface on nano-TiO_2. [Source: Ahmad and Aleem [11]].

In the studies conducted, the porosity of AE9342 was less than SM102, and also the bond strength of AE9342 was higher than the bond strength of SM102. Nanoparticles played a crucial role in controlling the corrosion mechanism. It has been shown by previous work on conducting surfaces (70Cu-30Ni) that nano zones are embedded in the homogeneous zones of nano melted particles in preventing the ingress of slurry and erosion-corrosion mechanism, both of which are responsible for increasing the resistance to erosion-corrosion. Microstructure holds

the key which depends on the reconstitution of powders and key APS parameters used in depositing the nanocoatings. The proposed mechanism of erosion-corrosion is shown in **Figure 34**.

The figure shows splats, inter-splat boundaries, pores, nano-agglomerates, and other features. It may be observed that the water passes through the inter-splat boundaries from various directions. The wide splat boundaries allow the ingress of water to the substrate resulting mainly in the formation of $Fe(OH)_2$, largely responsible for erosion-corrosion and builds up a fibrous network which allows dissolution by liquid metal ingress. The pores are wide to assist propagation of cracks. It is known that ductile materials have lesser erosion loss and offer an impingement angle relative to substrate, whereas the opposite is true of hard surface-coated samples. Stainless steel falls in this category. The coating of n-TiO2 is harder than the conventional TiO2-coated substrate. The nanostructure coatings have shown very lesser impingement angle compared to conventional coatings. This is exemplified by ball-valve application in harsh environment [18]. Very low pressure plasma spray offers advantages over the conventional air plasma spray because a fully developed nanostructured coating can be deposited which offers superior properties. However, the work conducted so far is not conclusive [19]. The corrosion resistance of nanostructured coating is clearly related to their morphology and adhesion of the nano-coating to the substrate. The mechanism suggested above is supported by SEM and AFM observations.

3. Conclusion

The resistance of nanostructured TiO_2 coating to erosion is controlled by the homogeneity and large fully melted zones of splats, homogeneous zone of nano-agglomerate particles, narrow interfacial boundaries, absence of fibrous network of dislodged particle of substrate, spherical splats, morphology, homogeneous distribution of splats, dense splats zone, embedding of nano zones in the coating with small variations in the surface roughness, which present the onset of localized corrosion and the deleterious effects caused by erosion-corrosion. It has been shown that plasma-sprayed nanostructured TiO_2 coatings offer a higher resistance to erosion-corrosion in 3.5 wt% NaCl aerated condition. The APS (Air Plasma Spray) coatings also offer high resistance to corrosion in salt spray chambers. Electrochemical polarization data obtained is in full agreement with the immersion study. Electrochemical corrosion studies also show a high resistance of nano-TiO_2 PAS coatings compared to conventional TiO2 APS coatings. The nano-TiO2 coatings deposited by HVOF (High Velocity Oxyfuel) offer relatively higher resistance to corrosion compared to APS n-TiO_2 coatings. The processing techniques influence the microstructure and consequently increase the corrosion resistance. The success of nanostructured coating market can be judged from the projected growth of market to $9.7 billion per annum by 2025. This dramatic upward trend calls for greater cumulative efforts of global researchers to fulfill the demand and make the coatings cost-effective. Our finding clearly reveals the advantages offered by n-TiO2 air plasma coatings in harsh environment. A new mechanism of erosion-corrosion of n-TiO2-coated substrates has been suggested; however, a conclusive mechanism is yet to be worked out.

Author details

Zaki Ahmad*, Asad Ullah Khan, Robina Farooq, Tahir Saif and Naila Riaz Mastoi

*Address all correspondence to: drzakiahmad@ciitlahore.edu.pk

COMSATS Institute of Information Technology, Lahore, Pakistan

References

[1] E. Turunen, T. Varis, T.E. Gustafsson, J. Keskinen, T. Falt, S.-P. Hannula, "Parameter optimization of HVOF sprayed nanostructured alumina and alumina-nickel composite coatings", Surface Coatings and Technology, Vol. 200(16–17), 2006, 4987–4994.

[2] L. Leblanc, "Abrasion and sliding wear of nanostructured ceramic coatings", Thermal Spray 2003: Advancing the Science & Applying the Technology, C. Moreau and B. Marple (Eds.), ASM International, Materials Park, Ohio, USA, 2003, 291–299.

[3] R. Unger, "Comparison of thermal spray bond coats", Proceedings of the National Thermal Conference, ASM International, Materials Park, OH, USA, 1987, 365–376.

[4] D. Mardare, P. Hones, Optical dispersion analysis of TiO2 thin films based on variable angle spectroscopic elipsometry measurements. Materials Science and Engineering: B, Vol. 68, 1999, 42.

[5] A.R. Bally, E.N. Korobeinkova, P.E. Schmid, F. Levy, F. Bussy, Structural and Electrical properties of Fe- Doped TiO2 thin films. Journal of Applied Physics, Vol. 31, 1989, 1149.

[6] P. Bansal, N.P. Padture, A. Vasiliev, "Improved interfacial mechanical properties of Al_2O_3-13 wt% TiO_2 plasma-sprayed coatings derived from nano crystalline powders", Acta Materialia, Vol. 51, 2003, 2959–2970.

[7] V. Chawla, B.S. Sidhu, D. Puri, S. Prakash, "Performance of plasma sprayed nano-structured and conventional coatings", Journal of the Australian Ceramic Society, Vol. 44(2), 2008, 56–62.

[8] Z. Ahmad, M. Ahsan, "Corrosion studies on the plasma sprayed nanostructured titanium dioxide coating". Anti-Corrosion Methods and Materials, Vol. 56(4), 2009, 187–195.

[9] L.L. Shaw, D. Goberman, R. Ren, M. Gell, S. Jiang, Y. Wang, T.D. Xiao, P.R. Strutt, "The dependency of microstructure and properties of nano structured coatings on plasma spray conditions", Surface Coatings & Technology, Vol. 130, 2000, 1–8.

[10] P. Ctibor, K. Neufuss, P. Chraska, "Microstructure and abrasion resistance of plasma sprayed titania coatings", Journal of Thermal Spray Technology, Vol. 15(4), 2006, 689–694.

[11] Z. Ahmad, A.B.J. Aleem, Resistance of nanostructured titanium dioxide coatings to erosion corrosion, Tribology – Materials, Surfaces & Interfaces, Vol. 3(1), 2009, 41–48.

[12] ASTM Designation: NACE TM0169/G31 - 12a, Standard Guide for Laboratory Immersion Corrosion Testing of Metals, © NACE International/ASTM International, West Conshohocken, PA, USA, 2015.

[13] ASTM Designation: G59 - 97 (Reapproved 2014), Standard Test Method for Conducting Potentiodynamic Polarization Resistance Measurements, © ASTM International, West Conshohocken, PA, USA, 2014.

[14] ASTM Designation: B117 – 11, Standard Practice for Operating Salt Spray (Fog) Apparatus, © ASTM International, West Conshohocken, PA, USA, 2011.

[15] Z. Ahmad, M. Ahsan, "Environmental response of plasma sprayed nanostructured coatings". Advanced Materials Research, Vol. 32, 2008, 65–70.

[16] G. Montavon, S. Sampath, C.C. Berndt, H. Herman, C. Coddet, "Effects of vacuum plasma spray processing parameters on splat morphology", Journal of Thermal Spray Technology, Vol. 4(1), 1995, 67–74.

[17] Z. Shui, B. Wang, A. Levy, Erosion of protective coatings. Surface and Coatings Technology, Vol. 43/44, 1999, 859–874.

[18] J. Willams, G.E. Kim, J. Walker, "Ball valves with nanostructured titanium oxide coatings for high-pressure acid-leach service: development to application", Proceeding of Pressure Hydrometallurgy, 2004. Vol. 16 (1), 34-39.

[19] Y. Gao, Y. Zhao, D. Yang, J. Gao, "A novel plasma-sprayed nanostructured coating with agglomerated-unsintered feedstock", Journal of Thermal Spray Technology, 2015, DOI: 10.1007/s11666-015-0340-1. Vol 25, Issue 1-2, pp. 291-300.